Recent trends in the waviness of the Northern Hemisphere wintertime polar and subtropical jets

Jonathan E Martin[1]

[1]University of Wisconsin-Madison

November 21, 2022

Abstract

A feature-based metric of the waviness of the wintertime, Northern Hemisphere polar and subtropical jets is developed and applied to three different reanalysis data sets. The analysis first identifies a "core isertel" along which the circulation per unit length is maximized in the separate polar (315:330K) and subtropical (340:355K) jet isentropic layers. Since the core isertel is, by design, an analytical proxy for the respective jet cores, the waviness of each jet is derived by calculating a hemispheric average of the meridional displacements of the core isertel from its equivalent latitude - the southern extent of a polar cap whose area is equal to the area enclosed by the core isertel. Analysis of the seasonal average waviness over the time series of the various data sets reveals that both jets have become systematically wavier while exhibiting no trends in their average speeds. The waviness of each jet evolves fairly independently of the other in most cold seasons and the slow northward creep of the polar jet is statistically significant. Finally, comparison of the composites of the waviest and least wavy seasons for each species reveals that such interannual variability is manifest in familiar large-scale circulation anomalies.

PLAIN LANGUAGE SUMMARY

Among the most common structural features of the earth's atmosphere are the narrow, meandering ribbons of maximum wind speed known as the jet streams. On any given winter day, there are usually two such jet streams; one located at ~9 km (the polar jet) and another, further south, located at ~12 km (the subtropical jet). These jet streams are both important weather producing features as well as influential governors of regional climate. This study considers trends in the wintertime waviness of the two jets as portrayed in three different data sets with long time series. The analysis reveals three important results. First, the waviness of both jets has been systematically increasing since ~1960. Second, despite their increasing waviness, the maximum speed of both jets has hardly changed. Third, the polar jet has been creeping slowly, but persistently, poleward over the last several decades. All three of these results are consistent with predictions that have recently been made about the behavior of the jets in a warmer climate and thus offer observational support for these forecasts.

RECENT TRENDS IN THE WAVINESS OF THE NORTHERN HEMISPHERE WINTERTIME POLAR AND SUBTROPICAL JETS

by

JONATHAN E. MARTIN

Department of Atmospheric and Oceanic Sciences
University of Wisconsin-Madison
1225 W. Dayton St.
Madison, WI 53706
608-262-9845
jemarti1@wisc.edu

Submitted for publication to *Journal of Geophysical Research:Atmospheres*
August 14, 2020

KEY POINTS

• The tropopause-level, polar and subtropical jet streams are becoming increasingly wavy during NH winter.

• Despite the increase in waviness, the speed of the jets has remained nearly constant.

• The polar jet is slowly, but systematically, creeping poleward in accord with climate model projections.

ABSTRACT

A feature-based metric of the waviness of the wintertime, Northern Hemisphere polar and subtropical jets is developed and applied to three different reanalysis data sets. The analysis first identifies a "core isertel" along which the circulation per unit length is maximized in the separate polar (315:330K) and subtropical (340:355K) jet isentropic layers. Since the core isertel is, by design, an analytical proxy for the respective jet cores, the waviness of each jet is derived by calculating a hemispheric average of the meridional displacements of the core isertel from its equivalent latitude - the southern extent of a polar cap whose area is equal to the area enclosed by the core isertel. Analysis of the seasonal average waviness over the time series of the various data sets reveals that both jets have become systematically wavier while exhibiting no trends in their average speeds. The waviness of each jet evolves fairly independently of the other in most cold seasons and the slow northward creep of the polar jet is statistically significant. Finally, comparison of the composites of the waviest and least wavy seasons for each species reveals that such interannual variability is manifest in familiar large-scale circulation anomalies.

1. Introduction

Among the most ubiquitous structural features of the Earth's atmosphere are the narrow, tropopause-level wind speed maxima known as jet streams or jets. These jets, often found nearly girdling the globe while exhibiting large meridional meanders, are the primary phenomena at the interface between synoptic-scale weather systems and the large-scale circulation. Consequently, they play a substantial role in the production of sensible weather in the mid-latitudes while serving as particularly influential governors of regional climate. Decades of observational work has identified two main varieties of jets, distinguished by their underlying dynamical origins. The polar jet (POLJ) forms as a result of eddy momentum flux convergence associated with the development of mid-latitude baroclinic waves (e.g. Held 1975; Rhines 1975; Panetta 1993) and is connected, via the thermal wind relationship, to the troposphere-deep baroclinicity of the middle latitudes. The subtropical jet (STJ) forms in response to angular momentum transport by the thermally direct Hadley circulation (Held and Hou 1980) and is, therefore, tied to the poleward edge of the tropical Hadley Cell. As a consequence of their different origins, the POLJ and STJ are often widely separated by latitude as well as elevation. The Northern Hemisphere (NH) jet stream has centers of maximum intensity located over the western Atlantic and western Pacific Oceans with the wintertime Pacific jet extending from East Asia to the date line. Unlike the Atlantic jet, the wintertime Pacific jet is regularly characterized by a collocation (or vertical superposition) of POLJ and STJ components and thus is often a hybrid feature (e.g. Christenson et al. 2017).

Both species of jets reside near the tropopause – the thermodynamic boundary that separates the stratosphere from the troposphere. The tropopause is characterized by strong first

77 order discontinuities in static stability, the mixing ratios of certain chemical constituents, as well
78 as potential vorticity (PV). Importantly, the tropopause does not occur at a uniform height over
79 the entire hemisphere nor does it exhibit a monotonic slope with latitude. Instead, as first
80 identified by Defant and Taba (1957), there is generally a three-step structure in tropopause
81 height from equator-to-pole with local regions of steep slope occurring at successively lower
82 elevation with increasing latitude.

83 These local maxima in slope are also regions of large PV gradient on isentropic surfaces.
84 This PV gradient serves as the restoring force for Rossby waves, the ubiquitous, planetary-scale
85 ridge-trough couplets that are primarily responsible for the production of organized weather
86 systems in the extratropics. Morgan and Nielsen-Gammon (1998) demonstrated the utility of
87 maps of θ and wind speed on the so-called dynamic tropopause (defined as a surface of constant
88 Ertel (1942) PV) for diagnosing weather systems. In this framework, the maxima in tropopause
89 slope become regions of large PV gradient on isentropic (potential temperature, or θ) surfaces, or
90 large θ gradient on isertelic (constant PV) surfaces, and are theoretically (Hoskins et al. 1985,
91 Cunningham and Keyser 2004) and empirically (Hoskins and Berrisford 1988, Davies and Rossa
92 2008) linked to the tropopause-level jet cores.

93 The behavior of the jets in a warmer climate has been a topic of considerable research
94 effort recently. The consensus view is that a robust poleward displacement of the jet axes will
95 likely characterize a warmer world (e.g. Yin 2005, Miller et al. 2006, Swart and Fyfe 2012,
96 Woollings and Blackburn 2012, Barnes and Polvani 2013). In addition, attempts have been
97 made, by various methods, to assess the waviness of the mid-latitude flow containing the jets.
98 Particularly at issue in recent years has been attribution of any such changes to the enhanced
99 lower tropospheric warming at high latitudes known as Arctic amplification (Serreze et al. 2009,

100 Screen and Simmonds 2010 and 2013, Francis 2017, Francis et al. 2018, Vavrus 2018). Nearly
101 all such attempts have employed analysis metrics involving geopotential height contours or
102 horizontal wind components in the middle and upper troposphere (e.g. Francis and Vavrus 2012
103 and 2015, Barnes 2013, Chen et al. 2015, DiCapua and Coumou 2016, Martineau et al. 2017).
104 However, considered from a PV perspective, the flow at 500 hPa is often strongly influenced by
105 near surface thermal contrasts (i.e. dynamically equivalent to low-level PV gradients following
106 Bretherton (1966)), internal diabatic processes and tropopause-level PV anomalies (Hoskins et
107 al. 1985, Davis and Emanuel 1991). Thus, though the 500 hPa flow often exhibits similarities to
108 the jet stream flows at higher altitudes, because it is shaped by these lower tropospheric and
109 diabatic influences to a greater extent than the tropopause-level flow, it might be expected that
110 tropopause-level jet waviness would differ noticeably from that of the mid-troposphere.
111 Consistent with this presumption and, despite a number of recent innovations in objective
112 identification of the jet streams themselves (e.g. Schiemann et al. 2009, Manney et al. 2011,
113 Limbach et al. 2012, Christenson et al. 2017), agreement on whether or not substantial changes
114 in jet waviness have been detected does not yet exist (Barnes and Screen, 2015). Underlying this
115 lack of consensus is the absence of a robust method of assessing the waviness of the tropopause-
116 level jets. Without regard to the question of possible links to Arctic amplification, the goals of
117 the present paper are limited to describing a method for separately quantifying the waviness of
118 the subtropical and polar jets and examining recent trends in both.
119 The paper is organized as follows. A theoretical and observational background to the
120 methodology used in the study is given in Section 2 along with a description of the data sets
121 used. In Section 3 aspects of the long-term trend and interannual variability of the waviness of
122 the Northern Hemisphere, cold-season subtropical and polar jets are considered. Included here

123 are analyses of the differences in the composite, large-scale dynamic and kinematic structures
124 associated with the waviest and least-wavy cold seasons in both species of tropopause-level jets.
125 A summary and conclusions, including suggestions for future work, are offered in Section 4.
126
127 **2. Data and Methodology**
128
129 In this study, the waviness of the two species of tropopause-level jets is assessed in the
130 context of understanding their relationships to the gradient of PV in prescribed isentropic layers.
131 Christenson et al. (2017) presented an objective method for identification of the separate polar
132 and subtropical jets in θ/PV space. They argued that the Northern Hemisphere cold season
133 (NDJFM) polar (subtropical) jet core lies on the equatorward, or low PV, edge of a strong PV
134 gradient in the 315:330 K (340:355K) isentropic layer. Justification for the PV gradient/jet
135 relationship follows from consideration of the quasi-geostrophic potential vorticity (QGPV)
136 following Cunningham and Keyser (2004). Recalling that QGPV is given by

137 $$q_g = \frac{1}{f_o}\nabla^2\phi + f + \frac{\partial}{\partial p}\left(\frac{f_o}{\sigma}\frac{\partial \phi}{\partial p}\right) = \Lambda(\phi) + f$$
138
139 (where $\Lambda = \frac{1}{f_o}\nabla^2 + \frac{\partial}{\partial p}\left(\frac{f_o}{\sigma}\right)\frac{\partial}{\partial p} + \frac{f_o}{\sigma}\frac{\partial^2}{\partial p^2}$ and ϕ is the geopotential), the cross-jet gradient of QGPV
140 ($\frac{\partial q_g}{\partial n}$ where $\hat{n}$ is the cross-flow direction in natural coordinates) can be expressed as
141 $$\frac{\partial q_g}{\partial n} = \Lambda\left(\frac{\partial \phi}{\partial n}\right) = \Lambda(-fV_g) \qquad (1)$$
142
143 after substituting from the natural coordinate expression for the geostrophic wind. Thus, local
144 maxima in the cross-flow gradient of QGPV are collocated with maxima in the geostrophic wind
145 speed. The analysis of Davies and Rossa (1998) offers empirical justification for confident
146 extension of this relationship to gradients in Ertel (1942) PV.

147 In the foregoing analysis we employ the zonal (*u)* and meridional (*v)* winds as well as
148 temperature (*T)* at 6h intervals from three different reanalysis data sets: NCEP/NCAR, JRA-55
149 and ERA5 reanalyses. We use 66 winters (1948 to 2013) of National Centers for Environmental
150 Prediction (NCEP) – National Center for Atmospheric Research (NCAR) reanalysis. The
151 NCEP-NCAR reanalysis data are available at 17 isobaric levels to 10 hPa on a 2.5° latitude-
152 longitude grid (Kalnay et al. 1996; Kistler et al. 2001). We employ 60 winters (1958-2017) of
153 the Japanese 55-year (JRA-55) reanalysis with data on 60 vertical levels up to 0.1 hPa on a
154 horizontal grid mesh of ~55 km (Kobayashi et al. 2015). The ERA5 data are on 137 vertical
155 levels from the surface to 80 km with grid spacing at ~31 km covering the period from 1979-
156 2018 (Copernicus Climate Change Service, CS3, 2017). As will be shown presently, the analysis
157 method involves assessment of the circulation which requires calculation of contour length.
158 Consequently, fair comparison among the data sets is best made by adopting a uniform
159 horizontal grid spacing. Therefore, all three data sets were bilinearly interpolated onto isentropic
160 surfaces at 5-K intervals (from 300 to 370 K) and 2.5° latitude-longitude grid spacing using
161 programs within the General Meteorological Analysis Package (GEMPAK) (desJardins et al.
162 1991). The average PV and average zonal and meridional wind speeds in both the polar jet
163 (315:330 K) and subtropical jet (340:355K) layers were then calculated four times daily for
164 every day in the trio of time series.
165 By virtue of the fact that the jets are always located in a region of strong PV gradient, a
166 reasonable proxy for the axis of maximum wind speed (or "core") of each jet is, on any given
167 day, one of several isertels within the strong gradient region. We shall refer to this particular
168 isertel as the "core isertel" and note here that it need not have the same value from one day to the
169 next. We seek to quantify the daily departure from zonality of such core isertels in each jet layer

as a means of directly assessing the waviness of the jet. In order to perform this analysis, we first consider the circulation

$$C = \oint \vec{U} \cdot \overrightarrow{dl}$$

along isertels ranging from 0.5 to 5.0 PVU (at 0.1 PVU intervals, 1 PVU = 10^{-6} m^2 K kg^{-1} s^{-1}) in each jet layer on every day in each time series. The core isertel in each layer on a given day is the isertel along which the average $|\vec{U}|$ per unit length is maximized. Examples illustrating the utility of this method for identifying the meandering cores of the subtropical and the polar jets are provided in Figs. 1 and 2, respectively. Note that the "stray" jet core in Fig. 1d, an isolated wind speed maxima far removed from the core isertel in the subtropical (340:355 K) layer, is actually the vertical extension of an obvious polar jet core in the underlying 315:330 K layer (Fig. 2d). Conversely, the "stray" wind speed maxima over the Middle East and the Himalaya in Fig. 2d is the lower portion of the subtropical jet core, identified in the 340:355 K layer (Fig. 1d). Throughout the time series, a large fraction of such seemingly disconnected isotach maxima in either layer can be accounted for in a similar fashion.

As stated earlier, the core isertel is not the same for each day in a given time series nor is it necessarily the same among the data sets on a given day that might be shared by the three time series. Consequently, its distribution in each jet layer in each data set is worthy of additional analysis. Figure 3 portrays the cumulative distribution functions for the core isertels of both the subtropical and polar jets in each of the three reanalysis data sets. The core isertel of the STJ layer peaks between 2.0 and 2.4 PVU across the three different data sets with the distribution both widening and shifting toward slightly higher isertelic values from NCEP to JRA-55 and again to ERA5 (Fig. 3a). Considering all three data sets, 79.4% of all DJF days exhibit a core isertel between 1 and 3 PVU in the STJ layer. The polar jet distribution is shifted toward lower

194 PV values (Fig. 3b) consistent with the concept of a "dynamically relevant PV contour" as
195 described by Kunz et al. (2015). A similar widening, but less shifting, of the distributions is seen
196 in this layer where the three data sets exhibit a remarkable similarity in the peak of their core
197 isertelic distributions. Overall, 83.6% of all DJF days had a core isertel between 1 and 3 PVU in
198 the POLJ layer.

199 Once the core isertel on a given day in a given layer has been identified, the area enclosed
200 by that contour is calculated. Next, its equivalent latitude – the southern extent of a polar cap
201 whose area is equal to the area enclosed by the core isertel – is computed. If A is the area
202 enclosed by the core isertel at a given time, then the equivalent latitude, ϕ_e, is given by
203 $\phi_e = \arcsin\left[1 - \frac{A}{2\pi {R_e}^2}\right]$ where R_e is the radius of the Earth. The meridional displacement of the
204 core isertel from its equivalent latitude is then measured along each longitude line in the manner
205 illustrated in Fig. 4. For core isertels intersecting a longitude line at multiple points, only those
206 segments of that longitude line along which the PV is greater (less) than the core isertel value
207 south (north) of the equivalent latitude are counted. The average latitudinal displacement (ALD)
208 of a given core isertel is then the sum of the length of all such segments divided by the number of
209 longitude lines at the resolution of the data (e.g. $2\pi/2.5° = 144$ for the present analysis) and is
210 converted to degrees for illustration purposes. Note that a perfectly zonal core isertel (i.e. a
211 zonal jet) would have an ALD of 0.0 with larger numbers representing increasingly wavier jets.
212 As an example, the ALDs of the tropopause-level jets observed on 18 February 1998 were
213 3.129° for the STJ (Fig. 4a) and 8.893° for the POLJ (Fig. 4b).
214
215 **3. Analysis**
216

a. Seasonal averages

The seasonal average latitudinal displacement of each jet is calculated as a simple 90-day (no leap days) average of the daily ALD in each cold season. The results of this averaging are shown in Fig. 5 and it is immediately apparent that the polar jet is substantially wavier than its subtropical counterpart. Though characterized by considerable interannual variability, both jets exhibit an increase in seasonally averaged waviness over the combined time series with $p << 0.001$ for both time series (a one-sided Student's t-test was employed). The remarkable similarity in the three time series of each species testifies to the robustness of this measure of waviness given other differences among the data sets. For comparison, the waviness of the 500 hPa geostrophic flow from the NCEP time series was assessed by calculating the aggregate ALD of a set of 5 isohypses ranging from 576 to 528 dm (at 120 m intervals) chosen because they contain the maximum 500 hPa geostrophic wind throughout the cold season. The aggregate ALD is calculated by summing the ALD of each isohypse and dividing by 5. As seen in Fig. 6, employment of isohypses at 500 hPa as a means of assessing the waviness of the mid-latitude flow, as has recently been suggested by a number of studies (e.g. Francis and Vavrus 2012, Barnes 2013, Screen and Simmonds 2014, Overland et al, 2015, DiCapua and Coumou 2016), does not similarly testify to an increase in jet waviness. As suggested earlier, this incongruence is likely borne of the fact that lower tropospheric and diabatic processes exert a stronger influence on the flow at 500 hPa than at the tropopause.

Daily time series of the ALD of each jet in a single cold season can also be constructed and compared to one another, as shown, for example, in Fig. 7 for the winter of 1990/91. Of interest in the present study is whether or not, and to what extent, the waviness of the two jets varies together. For the example season of 1990/91 the correlation between the two time series

240 is quite low (r=0.2353 for NCEP, 0.2217 for JRA-55 and 0.2481 for ERA5). In fact, the lack of
241 even a modest correlation between the waviness of the two jets in a given cold season appears to
242 be the rule rather than the exception. The two time series are correlated with magnitudes less
243 than 0.3 in 50 of 66 NCEP cold seasons, 46 of 60 JRA-55 cold seasons and 32 of 40 ERA5 cold
244 seasons. Thus, despite synoptic evidence of episodic periods of substantial and impactful
245 interaction between them (e.g. Uccellini et al. 1984, Bosart et al. 1996, Winters and Martin
246 2014), it appears that throughout an average NH cold season the waviness of the two jet species
247 evolves with a fair degree of independence. This characteristic is likely reflective of the fact that
248 the two jets arise from quite different large-scale forcings.
249 The feature-based analysis method employed here to measure jet waviness relies upon
250 calculation of the circulation along a collection of tropopause-level isertels. As described earlier,
251 the isertel with the greatest circulation per unit length (e.g. the largest average $\vec{U}$) is deemed the
252 core isertel. Thus, the *average* $\vec{U}$ *along the core isertel* on any given day represents the average
253 jet speed for that species for that day. Time series of the seasonal average speeds of the
254 subtropical and polar jet cores from each of the three reanalyses are shown in Fig. 8. A couple of
255 characteristics of the analysis stand out. First, though the year-to-year variability in ERA5 is
256 identical to that displayed by the nearly coincident NCEP/JRA-55 data, for both the subtropical
257 and polar calculations, ERA5 data return lower values of the jet core speeds – by an average of
258 3.65 m s^{-1} for the STJ and 2.70 m s^{-1} for the POLJ. Second, focusing on the JRA-55 time series
259 of both jets, the trends are very small indicating increases of just 0.6 m s^{-1} for the STJ and 1.0. m
260 s^{-1} for the POLJ spread over 60 years with *p*-values of 0.1749 and 0.1483, respectively. Hoffman
261 et al. (2019) showed that the zonally averaged Northern Hemisphere jet in January 2017 was
262 slightly slower in ERA5 than in the ERA-Interim (their Figs. 3 and 4). They suggested that the

higher spatial and temporal resolution of the ERA5 may account for the difference through improved representation of convective updrafts, gravity waves and other meso- to synoptic-scale features that can enhance mixing. The persistent discrepancy between the ERA5 and NCEP/JRA-55 jet core wind speeds in the present analysis may have similar origins.

Identification of the core isertel directly leads to calculation of the daily values of the equivalent latitude, essentially the zonally averaged latitude, of each jet core. Thus, another intriguing by-product of the analysis is the construction of time series of seasonal average equivalent latitudes of the subtropical and polar jet cores. Such time series, from each of the three reanalyses, are shown in Fig. 9. The trend lines through each time series are derived from the 60-year JRA-55 data. Very little change is suggested in the seasonally averaged latitude of the STJ (0.4° poleward increase over 60 years, $p = 0.222$). The polar jet, however, has crept northward at triple that rate and its trend line has a p-value of 0.008. Trend lines for the NCEP and ERA5 POLJs have p-values of 0.003 and 0.030, respectively.

b. Impact of variability in jet waviness on Northern Hemisphere wintertime circulation

Using the daily time series from each season, such as that in Fig. 7, it is possible to identify the waviest and least wavy seasons for each jet species by simply summing the daily departures from average over the 90 days of each cold season. The list of integrated seasonal departures from average waviness for each species from each data set (for the overlapping years only) is shown in Table 1. From this list, the five waviest and five least wavy seasons for each species were identified. Composites of several variables from the waviest and least wavy POLJ

285 and STJ seasons thus selected were constructed. In the subsequent analysis we show differences
286 in each variable obtained by subtracting the least wavy from the waviest composite.

287 Figure 10a shows the 1000 hPa geopotential height differences between seasons with the
288 waviest and least wavy polar jets. Wavy polar jet seasons are attended by height anomalies
289 reminiscent of the positive North Atlantic Oscillation (NAO) in the north Atlantic (Fig. 10a). The
290 height differences that exist between extremes of waviness of the subtropical jet share this
291 positive NAO signal while exhibiting much more robust anomalous ridging centered on the Gulf
292 of Alaska and extending from the west coast of North America to the dateline (Fig. 10b).

293 Related to these lower tropospheric height differences are differences in the 300 hPa
294 zonal wind. In the north Atlantic the wavy polar jet seasons are characterized by a poleward
295 displacement of the jet axis and a weakening of the zonal wind in a band stretching across the
296 basin from the Carolina coast to Iberia and the Mediterranean. In the Pacific basin, wavy polar
297 jet years appear to have little influence on the Pacific jet along nearly the length of its
298 climatological axis (Fig. 11a). The influence of subtropical jet variability on the circulation
299 changes in the north Atlantic is quite similar while in the Pacific basin wavy subtropical jet
300 seasons encourage a poleward displacement of the jet over the Bering Sea and Gulf of Alaska
301 and a broadly weaker flow equatorward of the climatological jet position in the central Pacific
302 (Fig. 11b). Such a distribution of anomalies is similar to that associated with north Pacific jet
303 retractions (Jaffe et. al 2011) which represent one phase of the leading mode of jet variability in
304 the basin (Athanasiadis et al. 2010).

305 The circulation differences engendered by the inter-seasonal variability in jet waviness
306 are apparently not confined to the troposphere. Associated modulations to the lower
307 stratospheric polar vortex are illustrated in Fig. 12. Wavy polar jet years are associated with an

intensified polar vortex over the Canadian Archipelago rung by light height rises at middle latitudes (Fig. 12a). Lower stratospheric circulation changes arising from inter-seasonal variation in the waviness of the subtropical jet are quite different with the vortex core displaced much farther west in wavy STJ years while pronounced ridging occurs over Scandinavia (Fig. 12b).

4. Summary

The analysis presented here focuses on observed morphological aspects of the Northern Hemisphere tropopause-level jet streams during boreal winter (DJF) as portrayed in three different reanalysis data sets covering parts of the last six and a half decades. Based upon the definitions of the polar and subtropical jets offered by Christensen et al. (2017), the analysis identifies a "core isertel" along which the circulation per unit length is maximized in the separate polar (315:330K) and subtropical (340:355K) isentropic layers for each day in the three time series. Such a core isertel represents an analytical proxy for the respective jet cores. Calculation of the hemispheric average latitudinal displacement of the core isertel from its equivalent latitude is, therefore, a robust, feature-based metric of the waviness of each species of jet. The analysis reveals that both jets are becoming systematically wavier while exhibiting no trends in their average speeds. Examination of the daily time series of waviness of the two jets strongly suggests that one's undulatory nature develops largely in isolation from the other. Additionally, while both jet cores are creeping toward the pole over time, only the POLJ encroachment, at three times the rate of the STJ, is statistically significant.

330 The poleward shift of the POLJ revealed here is consistent with observations of
331 systematic poleward shifts in mid-latitude cloud fields over the past several decades as shown in
332 the analyses of Bender et al. (2012), Eastman and Warren (2013) and Norris et al. (2016).
333 Additionally, modelling evidence suggests that increasing greenhouse gases will force the NH
334 mid-latitude jet poleward in the 21st century (e.g., Barnes and Polvani 2013, Simpson et al.
335 2014). In fact, in their analysis of CMIP5 model output, Barnes and Polvani (2013) found that
336 the NH jet shifted ~1° poleward by the end of the century while its core speed remained constant.
337 Such behavior is consistent with the results of the present observational analysis.
338 Though the aim of this study is to document, rather than diagnose, increasing jet
339 waviness, prior work has considered the dynamical interaction between increased waviness and
340 poleward migration of the jets. A number of investigators (e.g. Thorncroft et al. 1993; Benedict
341 et al. 2004; Rivière and Orlanski 2007; Martius et al. 2007; Strong and Magnusdottir 2008;
342 Woollings et al. 2008; Rivière 2009) have examined the poleward momentum flux characteristic
343 of certain configurations of the large scale flow. These analyses have concluded that individual
344 synoptic-scale eddies can play an important role in the formation of large-scale flow anomalies
345 through wave breaking. Vallis and Gerber (2008) have suggested that high impact
346 teleconnections such as the North Atlantic Oscillation (NAO), the Pacific North America pattern
347 (PNA) and the annular modes are fundamentally related to fluctuations in the latitude and
348 amplitude of the tropopause-level jets. Introduction of the LC1/LC2 life cycle dichotomy by
349 Thorncroft et al. (1993) represented a recognition that anticyclonic (LC1) and cyclonic (LC2)
350 wave breaking lay at the heart of the interaction of eddies with the larger scale flow. When
351 anticyclonic wave breaking occurs near the jet core, the jet is pushed poleward in response to the
352 associated distribution of momentum fluxes. Framed in terms of the PV gradient, Rivière (2009)

353 concluded that a higher latitude jet is more likely to experience anticyclonic wavebreaks which
354 would, in turn, encourage further poleward displacement. If the increased waviness reported
355 here has been manifest as an increase in the frequency of positively tilted waves, then the
356 attendant poleward migration of the jets may bear a direct dynamical link to the waviness.
357 Examination of this potential connection, dependent on construction of an objective method for
358 identifying the tilt of the waves, following the work of Wernli and Sprenger (2007) and Martius
359 et al. (2008), is a subject of ongoing research.

360 Equally unknown in the wake of the present analysis is the role of the tropics in forcing
361 the observed increased waviness of the subtropical jet. A recent analysis of the subtropical jet by
362 Martius (2014) considered the interaction of the tropics and extratropics with the jet from the
363 perspective of trajectory analysis. She showed that air parcels that ended up in the jet over
364 Africa (East Asia/western Pacific) ascended over South America (Indian Ocean and the Maritime
365 Continent) before following an anticyclonic path toward the jet. The analysis showed that the
366 wintertime Hadley circulation is zonally asymmetric connecting tropical convection in localized
367 regions to segments of the jet. Whether or not the increased waviness of the subtropical jet is
368 directly related to changes in such tropical convective forcing is not known though a recent
369 analysis by Röthlisberger et. al (2018) suggests a connection.

370 The analysis methodology introduced here has been applied hemispherically but could
371 equally be employed in regional analyses. Such a regional analysis of the 500 hPa flow over
372 North America and its relation to Arctic amplification and hemispheric snow cover was recently
373 performed by Vavrus et al. (2017). A primary motivation for shrinking the analysis domain was
374 their suspicion that doing so would enhance the strength of the desired signal. Indeed, DiCapua
375 and Coumou (2016) found that regional trends in their meandering index were 2 to 3 times larger

than those observed over the full hemisphere. Tracking regional trends in the average latitudinal displacement of the core isertel would identify which regions are most strongly contributing to the hemispheric trend identified here. Such an analysis would likely also provide a more detailed sense of the physical connections between the parade of weather systems and the increased waviness of the jets.

Finally, use of reanalysis data sets to determine climatological trends can be problematic for a number of reasons including changing data types and volumes as well as biases in assimilation systems as suggested by Bengtsson et al. (2004). The results presented here rely on application of an analysis scheme to three quite different reanalysis data sets, each with its own advantages and disadvantages. The remarkably similar signals arising from these heterogeneous inputs suggests a robustness to the underlying signal that this analysis has sought to uncover. A convincing alternative assessment of these results would result from applying the same analysis method to output from 20th century GCM runs in the CMIP5 or CMIP6 suites. Such work is currently ongoing.

ACKNOWLEDGEMENTS: This work was supported by the National Science Foundation under grant ATM-1265182. NCEP Reanalysis data provided by the NOAA/OAR/ESRL PSL, Boulder, CO and available at https://psl/noaa.gov/. JRA-55 data available from the Research Data Archive at the National Center for Atmospheric Research. ERA5 data available at Copernicus Climate Change Service Climate Data Store (CDS), https://cds.climate.copernicus.eu/cdsapp#!/home. The author wishes to thank Profs. Michael Morgan, Stephanie Henderson, Andrew Winters, and Gary Lackmann for helpful comments and

398 suggestions. Dr. Brett Hoover, Dr. Melissa Breeden and Mr. Patrick Beaty are also gratefully
399 acknowledged.
400

401 REFERENCES

402

403 Athanasiadis, P. J., J. M. Wallace, and J. J. Wettstein, 2010: Patterns of wintertime jet stream
404 variability and their relation to the storm tracks. *J. Atmos. Sci.*, **67**, 1361–1381.

405

406 Barnes, E. A., 2013: Revisiting the evidence linking Arctic amplification to extreme weather in
407 midlatitudes. *Geophys. Res. Let*., **40**, 4734-4739.

408

409 _____, and L. Polvani, 2013: Response of the midlatitude jets, and of their variability, to
410 increased greenhouse gases in the CMIP5 models. *J. Climate*, **26**, 7117-7135.

411

412 _____, and J. A. Screen, 2015: The impact of Arctic warming on the midlatitude jet-stream: Can
413 it? Has it? Will it? *WIREs Clim Change*, **6**, 277–286. doi: 10.1002/wcc.337.

414

415 Bender, F.A., Ramanathan, V. & Tselioudis, G. Changes in extratropical storm track cloudiness
416 1983–2008: observational support for a poleward shift. *Clim Dyn* **38,** 2037–2053 (2012).
417 https://doi.org/10.1007/s00382-011-1065-6

418

419 Benedict, J., S. Lee, and S. Feldstein, 2004: Synoptic view of the North Atlantic Oscillation. *J.*
420 *Atmos. Sci*., **61**, 121–144.

421

Bengtsson, L., S. Hagemann, and K. I. Hodges, 2004: Can climate trends be calculated from reanalysis data? *JGR:Atmospheres*, **109**(D11), https://doi.org/10.1029/2004JD004536.

Bosart, L. F., G. J. Hakim, K. R. Tyle, M. A. Bedrick, W. E. Bracken, M. J. Dickinson, and D. M. Schultz, 1996: Large-scale antecedent conditions associated with the 12–14 March 1993 cyclone ("Superstorm '93") over eastern North America. *Mon. Wea. Rev.*, **124**, 1865-1891.

Bretherton, F. P., 1966: Critical layer instability in baroclinic flows. *Quart. J. Royal Meteor. Soc.*, **92**, 325–334.

Christenson, C. E., J. E. Martin, and Z. J. Handlos, 2017: A synoptic-climatology of Northern Hemisphere, cold season polar and subtropical jet superposition events. *J. Climate*, **30**, 7231-7246.

Copernicus Climate Change Service (C3S) (2017): ERA5: Fifth generation of ECMWF atmospheric reanalyses of the global climate. Copernicus Climate Change Service Climate Data Store (CDS), *March 2020,* https://cds.climate.copernicus.eu/cdsapp#!/home

Cunningham, P., and D. Keyser, 2004: Dynamics of jet streaks in a stratified quasi-geostrophic atmosphere: Steady-state representations. *Quart. J. Roy. Meteor. Soc.,* **130,** 1579-1609.

Davies, H. C., and A. M. Rossa, 1998: PV frontogenesis and upper-tropospheric fronts. *Mon. Wea. Rev.*, **126**, 1528-1539.

Davis, C. A., and K. A. Emanuel, 1991: Potential vorticity diagnostics of cyclogenesis. *Mon. Wea. Rev.*, **119**, 1929–1953

Defant, F., and H. Taba, 1957: The threefold structure of the atmosphere and the characteristics of the tropopause. *Tellus*, **9**, 259-275.

desJardins, M. L., K. F. Brill, and S. S. Schotz, 1991: Use of GEMPAK on UNIX workstations. Preprints, *Seventh Int. Conf. on Interactive Information and Processing Systems for Meteorology, Oceanography, and Hydrology*, New Orleans, LA, Amer. Meteor. Soc., 449–453.

DiCapua G., and D. Coumou,2016: Changes in the meandering of the Northern Hemisphere circulation. *Environ. Res. Lett.*, **11**, 094028, doi:10.1088/1748-9326/11/9/094028.

Eastman, R., and S. G. Warren, 2013: A 39-Yr survey of cloud changes from land stations worldwide 1971–2009: Long-term trends, relation to aerosols, and expansion of the tropical belt. *J. Climate*, **26**, 1286–1303, https://doi.org/10.1175/JCLI-D-12-00280.1.

Ertel, H., 1942: Ein Neuer hydrodynamischer Wirbelsatz. *Meteor. Z.*, **59**, 271-281.

Francis, J. A., and S. J. Vavrus, 2012: Evidence linking Arctic amplification to extreme weather in mid-latitudes. *Geophys. Res. Let.*, **39**, L06801, doi:10.1029/2012GL051000.

_____, and _____, 2015: Evidence for a wavier jet stream in response to rapid Arctic warming. *Environ. Res. Lett*. **10**, 014005, doi:10.1088/1748-9326/10/1/014005.

Held, I. M., 1975: Momentum transport by quasi-geostrophic eddies. *J. Atmos. Sci*., **32**, 1494-1497.

____, and A. Y. Hou, 1980: Nonlinear axially symmetric circulations in a nearly inviscid atmosphere. *J. Atmos. Sci*., **37**, 515-533.

Hoffman, L. G. Gunther, D. Li, O. Stein, X. Wu, S. Greissbach, Y. Heng, P. Konopka, B. Vogel, and J. S. Wright, 2019: From ERA-Interim to ERA5: The considerable impact of ECMWF's next-generation reanalysis on Lagrangian transport simulations. *Atm. Chem. and Physics*, **19**, 3097-3124.

Hoskins, B. J., M. E. McIntyre, and A. W. Robertson, 1985: On the use and significance of isentropic potential vorticity maps. *Quart. J. Roy. Meteor. Soc*., **111**, 877–946.

Jaffe, S. C., J. E. Martin, D. J. Vimont and D. J. Lorenz, 2011: A synoptic climatology of episodic, subseasonal retractions of the Pacific jet. *J. Climate*, **24**, 2846–2860.

Kalnay, E. and co-authors, 1996: The NCEP/NCAR 40-year reanalysis project. *Bull. Amer. Meteor. Soc*., **77**, 437-470.

Kistler, R. and co-authors, 2001: The NCEP-NCAR 50-Year reanalysis: Monthly means CD-ROM and documentation. *Bull. Amer. Meteor. Soc.*, **82**, 247-267.

Kobayashi, S., Y. Ota, Y. Harada, A. Ebita, M. Moriya, H. Onoda, K. Onogi, H. Kamahori, C. Kobayashi, H. Endo, K. Miyaoka, and K. Takahashi, 2015: The JRA-55 reanalysis: General specifications and basic characteristics. *J. Meteor. Soc. Japan*, **93**, 5-48.

Kunz, A., M. Sprenger, and H. Wernli, 2015: Climatology of potential vorticity streamers and associated isentropic transport pathways across PV gradient barriers, *J. Geophys. Res. Atmos.*, **120**, 3802–3821, doi:10.1002/2014JD022615.

Limbach, S., Schömer, E., and Wernli, H., 2002: Detection, tracking and event localization of jet stream features in 4-D atmospheric data, *Geosci. Model Dev.*, **5**, 457-470.

Manney, G. L., Hegglin, M. I., Daffer, W. H., Santee, M. L., Ray, E. A., Pawson, S., Schwartz, M. J., Boone, C. D., Froidevaux, L., Livesey, N. J., Read, W. G., and Walker, K. A.: Jet characterization in the upper troposphere/lower stratosphere (UTLS): Applications to climatology and transport studies. *Atmos. Chem. Phys.*, **11**, 6115–6137, doi:10.5194/acp-11-6115-2011.

Martius, O., 2014: A Lagrangian analysis of the Northern Hemisphere subtropical jet. *J. Atmos. Sci.*, **71**, 2354-2369.

_____, C. Schwierz, and H. Davies, 2007: Breaking waves at the tropopause in the wintertime Northern Hemisphere: Climatological analyses of the orientation and the theoretical LC1/2 classification. *J. Atmos. Sci*., **64**, 2576–2592.

_____, C. Scwierz, and H. C. Davies, 2008: Far-upstream precursors of heavy precipitation on the Alpine south-side. *Quart. J. Roy. Meteor. Soc*., **134**, 417-428.

Miller, R. L., G. A. Schmidt, and D. T. Shindell, 2006: Forced annular variations in the 20th century Intergovernmental Panel on Climate Change Fourth Assessment Report models. *J. Geophys. Res*., **111**, D18101, doi:10.1029/2005JD006323.

Morgan, M. C., and J. W. Nielsen-Gammon, 1998: Using tropopause maps to diagnose midlatitude weather systems. *Mon. Wea. Rev*., **126**, 2555-2579.

Overland, J., J. A. Francis, R. Hall, E. Hanna, S-J Kim, and T. Vihma, 2015: The melting Arctic and midlatitude weather patterns: Are they connected? *J. Climate*, **28**, 7917-7932.

Panetta, R. L., 1993: Zonal jets in wide baroclinically unstable regions: Persistence and scale selection. *J. Atmos. Sci*., **50**, 2073-2106.

Rhines, P. B., 1975: Waves and turbulence on a beta-plane. *J. Fluid Mech*., **69**, 417-443.

538 Rivière, G., 2009: Effect of latitudinal variations in low-level baroclinicity on eddy life cycles
539 and upper-tropospheric wave-breaking processes. *J. Atmos. Sci*., **66**, 1569-1592.
540
541 _____, and I. Orlanski, 2007: Characteristics of the Atlantic storm-track eddy activity and its
542 relation with the North Atlantic Oscillation. *J. Atmos. Sci*., **64**, 241–266.
543
544 Röthlisberger, M., O. Martius, and H. Wernli, 2018: Northern Hemisphere Rossby wave
545 initiation events on the extratropical jet – a climatological analysis. *J. Climate*, **31**, 743-
546 760.
547
548 Scheimann, R., D. Lüthi, and C. Schär, 2009: Seasonality and interannual variability of the
549 westerly jet in the Tibetan Plateau region. *J. Climate*, **22**, 2940-2957.
550
551 Serreze, M. C., A. P. Barrett, J. C. Stroeve, D. N. Kindig, and M. M. Holland, 2009: The
552 emergence of surface-based Arctic amplification, *The Cryosphere*, **3**, 11-19.
553
554 Simpson, I. R., T. A. Shaw, and R. Seager, 2014: A diagnosis of the seasonally longitudinally
555 varying midlatitude circulation response to global warming. *J. Atmos. Sci.*, **71**, 2489–
556 2515, https://doi.org/10.1175/JAS-D-13-0325.1.
557
558 Strong, C., and G. Magnusdottir, 2008: Tropospheric Rossby wave breaking and the NAO/NAM.
559 *J. Atmos. Sci*., **65**, 2861–2876.
560

561 Swart, N. C., and J. C. Fyfe, 2012: Observed and simulated changes in the Southern Hemisphere
562 surface westerly wind-stress. *Geophys. Res. Let.*, **39**, L16711,
563 doi:10.1029/2012GL052810.
564
565 Thorncroft, C. D., B. J. Hoskins, and M. McIntyre, 1993: Two paradigms of baroclinic-wave
566 life-cycle behaviour. *Quart. J. Roy. Meteor. Soc.*, **119**, 17–55.
567
568 Uccellini, L. W., P. J. Kocin, and R. A. Petersen, 1984: The Presidents' Day cyclone of 18–19
569 February 1979: Synoptic overview and analysis of the subtropical jet streak influencing
570 the pre-cyclogenetic period. *Mon. Wea. Rev.*, **112**, 31-55.
571
572 Vallis, G. K., and E. P. Gerber, 2008: Local and hemispheric dynamics of the North Atlantic
573 Oscillation, annular patterns and the zonal index. *Dyn. Atmos. and Oceans*, **44**, 184-212.
574
575 Vavrus, S. J., F. Wang, J. E. Martin, J. A. Francis, Y. Peings, and J. Cattiaux, 2017: Changes in
576 North American circulation and extreme weather: Influence of arctic amplification and
577 Northern Hemisphere snow cover. *J. Climate* , **30**, 4317-4333.
578
579 Wernli, H. and M. Sprenger, 2007: Identification and ERA-15 climatology of potential vorticity
580 streamers and cutoffs near the extratropical tropopause. *J. Atmos. Sci.*, **64**, 1569-1586.
581
582 Winters, A. C., and J. E. Martin, 2014: The role of a polar/subtropical jet superposition in the
583 May 2010 Nashville Flood. *Wea. Forecasting*, **29**, 954-974.
584

585 Woollings, T. and M. Blackburn, 2012: The north Atlantic jet stream under climate change and
586 its relation to the NAO and EA patterns. *J. Climate*, **25**, 886-902.
587
588 Woollings, T., B. Hoskins, M. Blackburn, and P. Berrisford, 2008: A new Rossby wave–
589 breaking interpretation of the North Atlantic oscillation. *J. Atmos. Sci*., **65**, 609–626.
590
591 Yin, J. H., 2005: A consistent poleward shift of the storm tracks in simulations of 21st century
592 climate. *Geophys. Res. Let.*, **32**, L18701,doi:10.1029/2005GL023684.
593
594
595
596
597
598
599
600

601
602

603
604 FIGURE CAPTIONS

605

606 **Fig. 1** Isotachs of the daily average wind speed (contoured every 10 m s^{-1} and shaded above 30
607 m s^{-1}) and the core isertel (bold solid line) in the 340:355 K isentropic layer on (a) 19 January
608 1958, (b) 26 December 1968, (c) 19 February 1979, and (d) 18 February 1998. The core isertel
609 has a value of 2.0 PVU in (a), 2.1 PVU in (b), 2.1 PVU in (c), and 1.4 PVU in (d). Blue dashed
610 line in (d) represents a portion of the axis of the polar jet on the same day in the 315:330 K
611 isentropic layer (see Fig. 2d and text for explanation).

612 **Fig. 2** Isotachs of the daily average wind speed (contoured every 10 m s^{-1} and shaded above 30
613 m s^{-1}) and the core isertel (bold solid line) in the 315:330 K isentropic layer on (a) 12 December
614 1954, (b) 8 January 1967, (c) 6 February 1978, and (d) 18 February 1998. The core isertel value
615 is 1.6 PVU in (a), 1.0 PVU in (b), 1.8 PVU in (c), and 2.2 PVU in (d). Red dashed line in (d)
616 represents a portion of the axis of the subtropical jet on the same day in the 340:355 K isentropic
617 layer (see Fig. 1d and text for explanation).

618 **Fig. 3** Cumulative distribution of core isertel value for each reanalysis time series in (a) the
619 340:355 K layer and (b) the 315:330 K layer. The dashed vertical lines indicate the peak value
620 of the core isertel in each layer from each data set. Isertel values given in potential vorticity
621 units (PVU, 1 PVU = 10^{-6} K m^2 kg^{-1} s^{-1}).

622

623 **Fig. 4** Schematic illustrating the concept of average latitudinal displacement (ALD) for (a) the
624 340:355 K layer and (b) the 315:330 K layer on 18 February 1998. Bold black line is the core
625 isertel in each layer (from the NCEP/NCAR Reanalysis), the gray dashed line is its equivalent

latitude, and the red and blue lines represent latitudinal displacements of the core isertel poleward and equatorward of the equivalent latitude, respectively. The ALD is the average of the sum of all such segments divided by the number of such segments available in the data set.

Fig. 5 Seasonal average ALD (in degrees) of the NH wintertime subtropical and polar jets for each cold season in the three reanalysis time series. The polar jet values are in the three shades of blue while the subtropical jet values are in the three shades of red. The thin black line through each time series represents the trend line for each (derived from the JRA-55 data) and is significant at the 99% level. The "YEAR" on the abscissa indicates the year in which December of that cold season occurred.

Fig. 6 Seasonal average aggregate ALD (in degrees) of a set of 5 isohypses at 500 hPa geopotential from the NCEP/NCAR reanalysis data. The thin dashed line is the trend line which is nearly flat and not statistically significant. For comparison, the light gray shading shows the same POLJ and STJ time series shown in Fig. 5. See text for additional explanation.

Fig. 7 Time series of the daily ALD of the polar (blue line) and subtropical (red lines) jets from each of the three data sets for the cold season 1990-91. The correlation between the two times series from each data set is indicated.

Fig. 8 Seasonal average **U** along the core isertel for the subtropical (red lines) and polar (blue lines) jets from each of the three reanalysis data sets. The light gray lines are trend lines for each time series from the JRA-55 data.

Fig. 9 Time series of the seasonal average equivalent latitude of the polar (blue lines) and subtropical (red lines) jets from the three different reanalysis data sets. The thin gray lines are the trend lines (from the JRA-55 data) which are small and only significant for the polar jet time series.

Fig. 10 1000 hPa height differences between composite waviest and least wavy (a) polar jet and (b) subtropical jet seasons constructed from the NCEP/NCAR reanalysis. See Table 1 for identification of the specific years comprising each composite. Positive (negative) height differences are in solid red (dashed blue) lines, labeled in m and contoured every 16m (-16m) beginning at 16m (-16m)

Fig. 11 300 hPa zonal wind differences between composite waviest and least wavy (a) polar jet and (b) subtropical jet seasons constructed from the NCEP/NCAR reanalysis. See Table 1 for identification of the specific years comprising each composite. Positive (negative) wind differences are in solid red (dashed blue) lines, labeled in m s^{-1} and contoured every 5 m s^{-1} (-5 m s^{-1}) beginning at 5 m s^{-1} (-5 m s^{-1}). Black dashed lines represent climatological axes of the DJF 300 hPa zonal wind.

Fig. 12 50 hPa height differences between composite waviest and least wavy (a) polar jet and (b) subtropical jet seasons constructed from the NCEP/NCAR reanalysis. See Table 1 for identification of the specific years comprising each composite. Positive (negative) height differences are in solid red (dashed blue) lines, labeled in m and contoured every 60m (-60m) beginning at 60m (-60m).

671

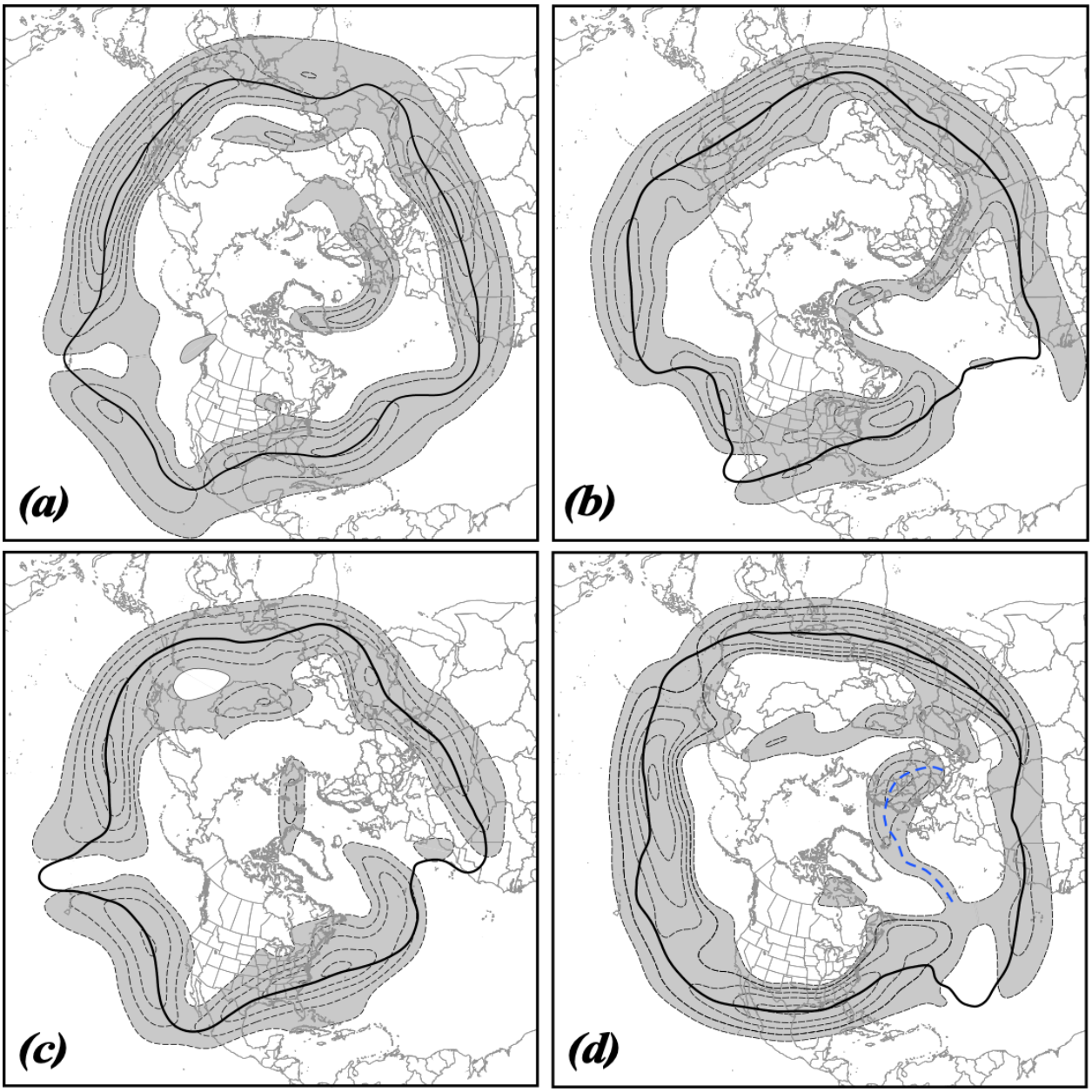

Fig. 1 Isotachs of the daily average wind speed (contoured every 10 m s^{-1} and shaded above 30 m s^{-1}) and the core isertel (bold solid line) in the 340:355 K isentropic layer on (a) 19 January 1958, (b) 26 December 1968, (c) 19 February 1979, and (d) 18 February 1998. The core isertel has a value of 2.0 PVU in (a), 2.1 PVU in (b), 2.1 PVU in (c), and 1.4 PVU in (d). Blue dashed line in (d) represents a portion of the axis of the polar jet on the same day
672 in the 315:330 K isentropic layer (see Fig. 2d and text for explanation).

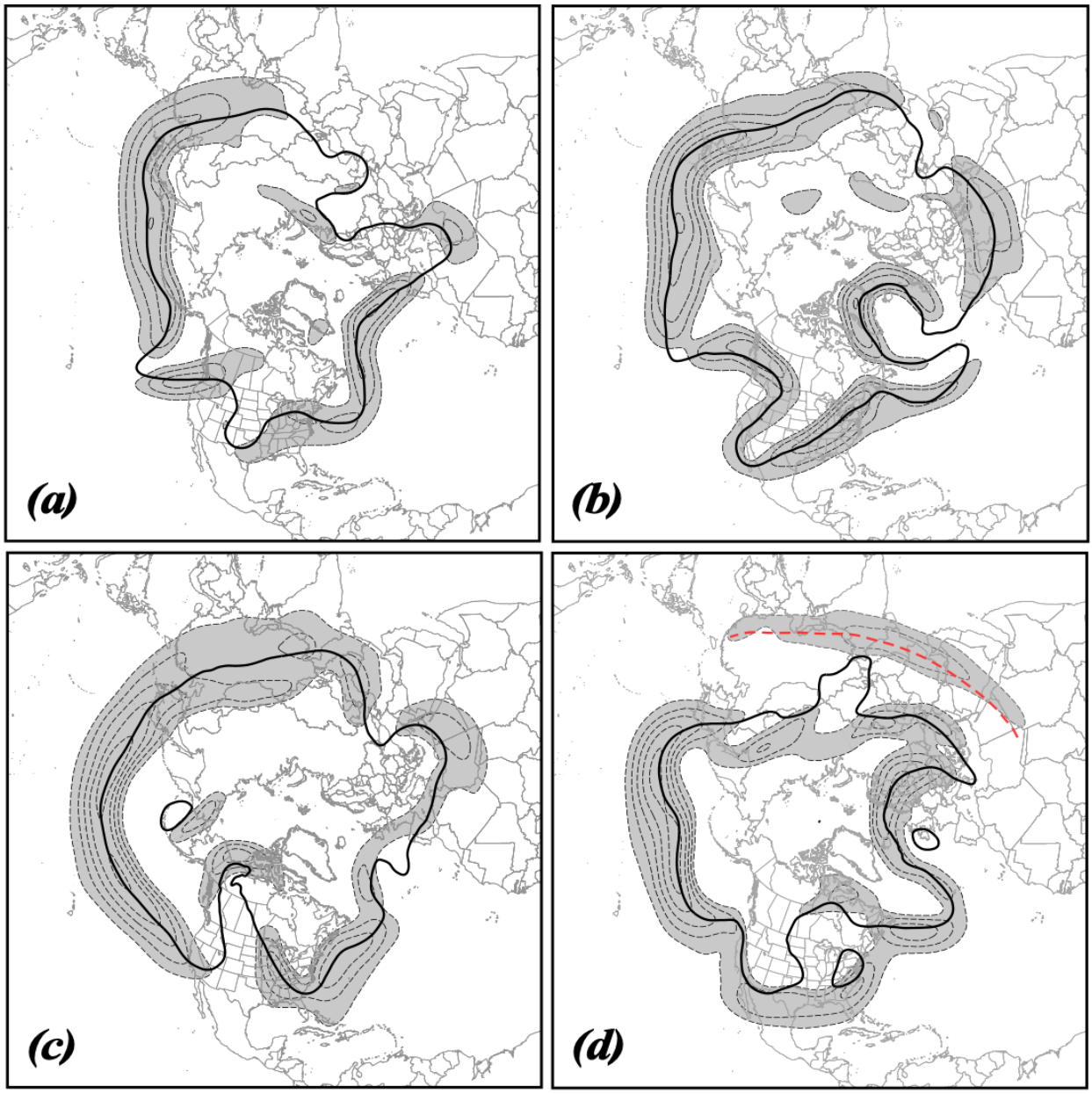

Fig. 2 Isotachs of the daily average wind speed (contoured every 10 m s^{-1} and shaded above 30 m s^{-1}) and the core isertel (bold solid line) in the 315:330 K isentropic layer on (a) 12 December 1954, (b) 8 January 1967, (c) 6 February 1978, and (d) 18 February 1998. The core isertel value is 1.6 PVU in (a), 1.0 PVU in (b), 1.8 PVU in (c), and 2.2 PVU in (d). Red dashed line in (d) represents a portion of the axis of the subtropical jet on the same day in the 340:355 K isentropic layer (see Fig. 1d and text for explanation).

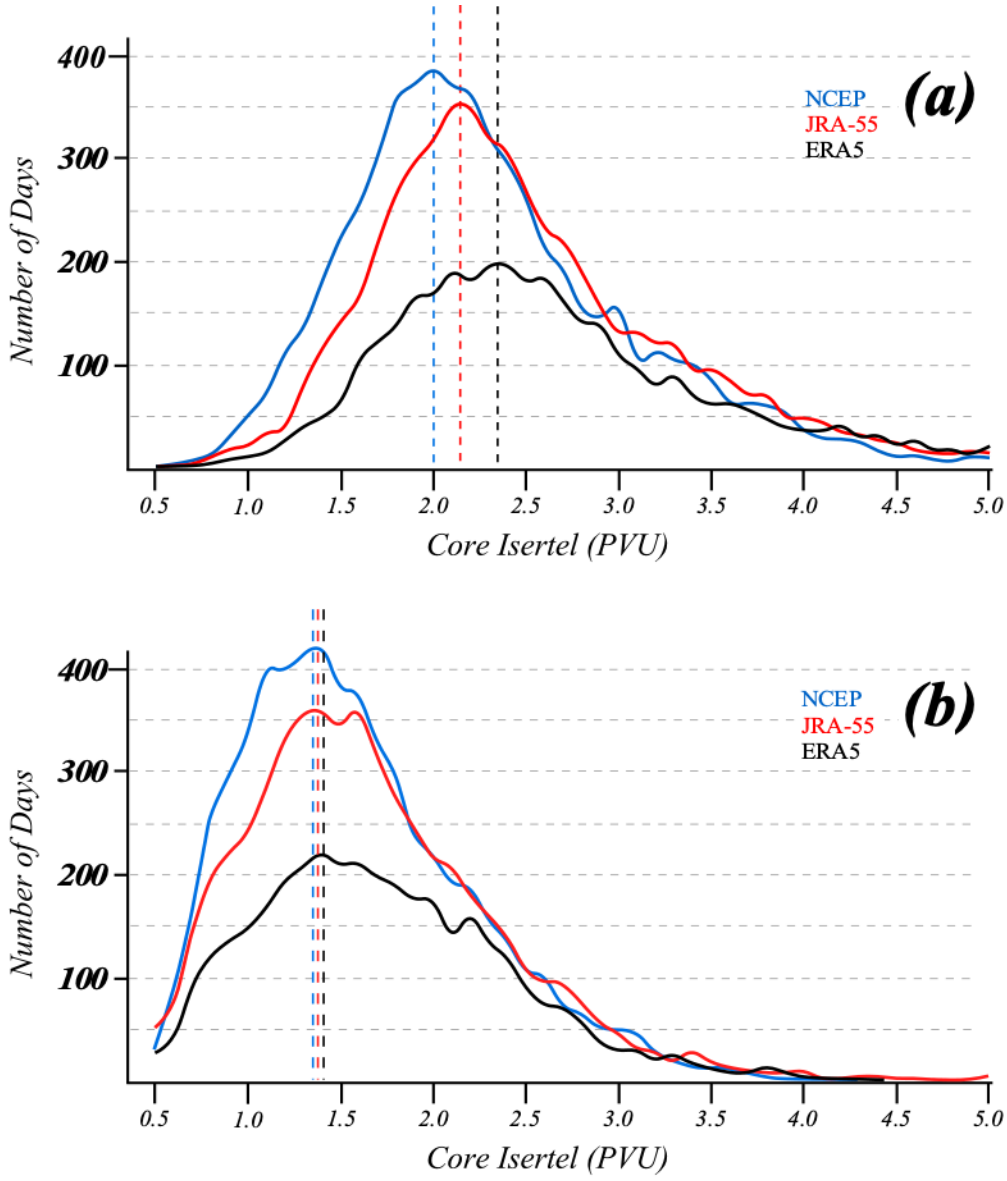

Fig. 3 Cumulative distriibution of core isertel value for each reanalysis time series in (a) the 340:355 K layer and (b) the 315:330 K layer. The dashed vertical lines indicate the peak value of the core isertel in each layer from each data set. Isertel values given in potential vorticity units (PVU, 1 PVU = 10^{-6} K m^2 kg^{-1} s^{-1}).

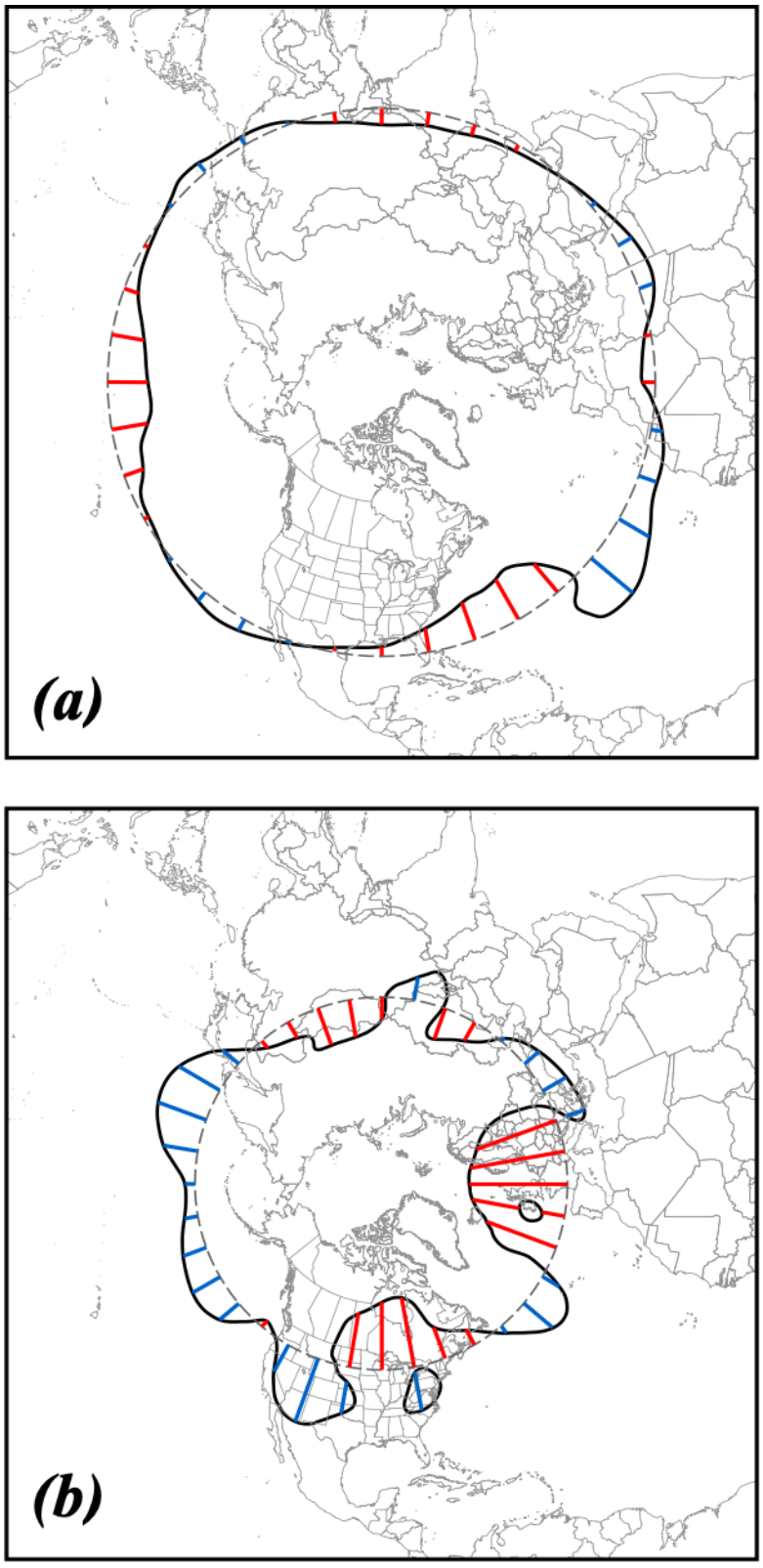

Fig. 4. Schematic illustrating the concept of average latitudinal displacement (ALD) for (a) the 340:355 K layer and (b) the 315:330 K layer on 18 February 1998. Bold black line is the core isertel in each layer (from the NCEP/NCAR Reanalysis), the gray dashed line is its equivalent latitude, and the red and blue lines represent latitudinal displacements of the core isertel poleward and equatorward of the equivalent latitude, respectively. The ALD is the average of the sum of all such segments divided by the number of such segments available in the data set.

677

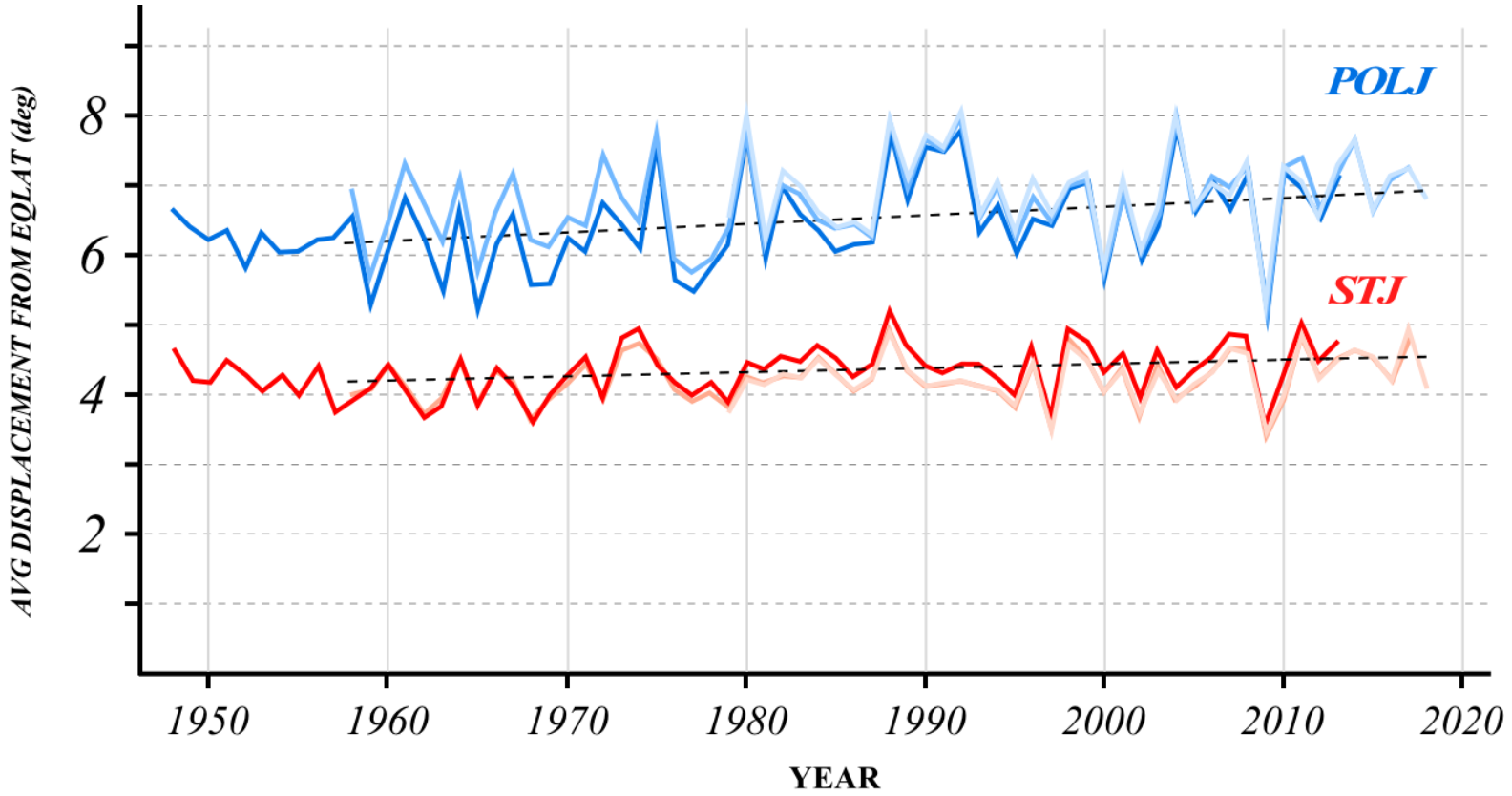

Fig. 5 Seasonal average ALD (in degrees) of the NH wintertime subtropical and polar jets for each cold season in the three reanalysis time series. The polar jet values are in the three shades of blue while the subtropical jet values are in the three three shades of red. The dashed black line through each time series represents the trend line for each (derived from the JRA-55 data) and is significant at the 99% level. The "YEAR" on the abscissa indicates the year in which December of that cold season occurred.

678

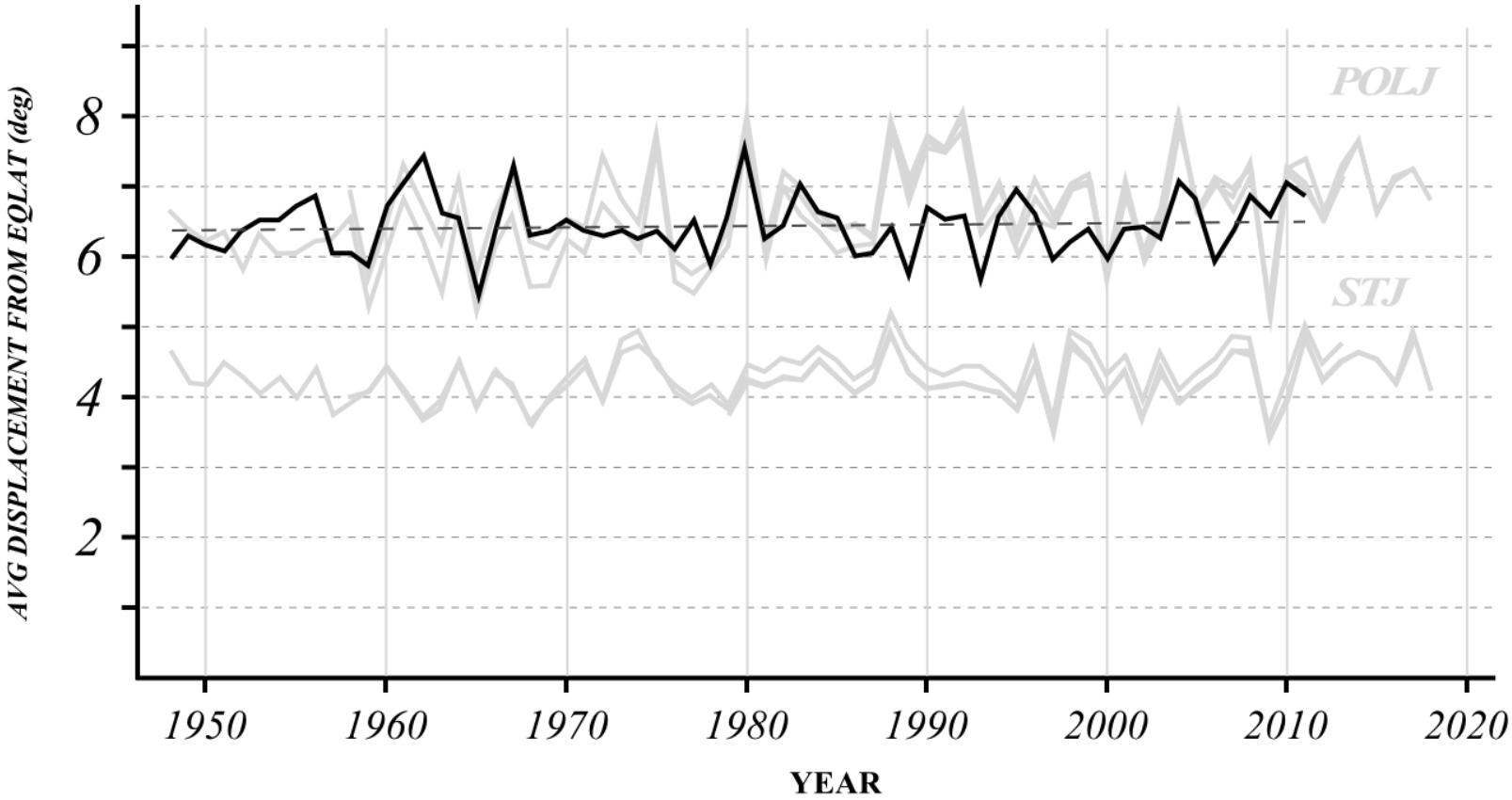

Fig. 6 Seasonal average aggregate ALD (in degrees) of a set of 5 isohypses at 500 hPa geopotential from the NCEP/NCAR reanalysis data. The thin dashed line is the trend line which is nearly flat and not statistically significant. For comparison, the light gray shading shows the same POLJ and STJ time series shown in Fig. 5. See text for additional explanation.

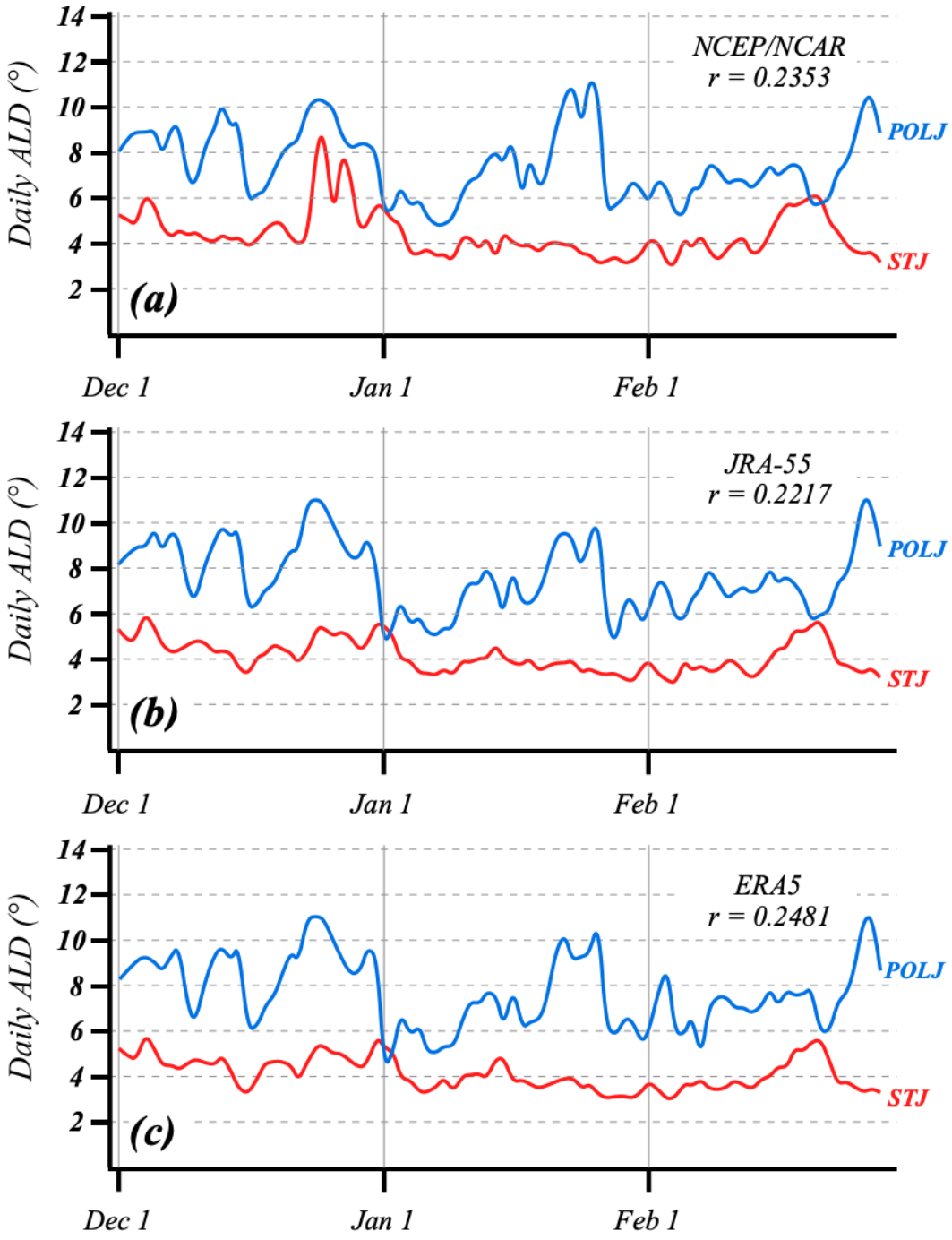

Fig. 7 Time series of the daily ALD of the polar (blue line) and subtropical (red lines) jets from each of the three data sets for the cold season 1990-91. The correlation between the two times series from each data set is indicated.

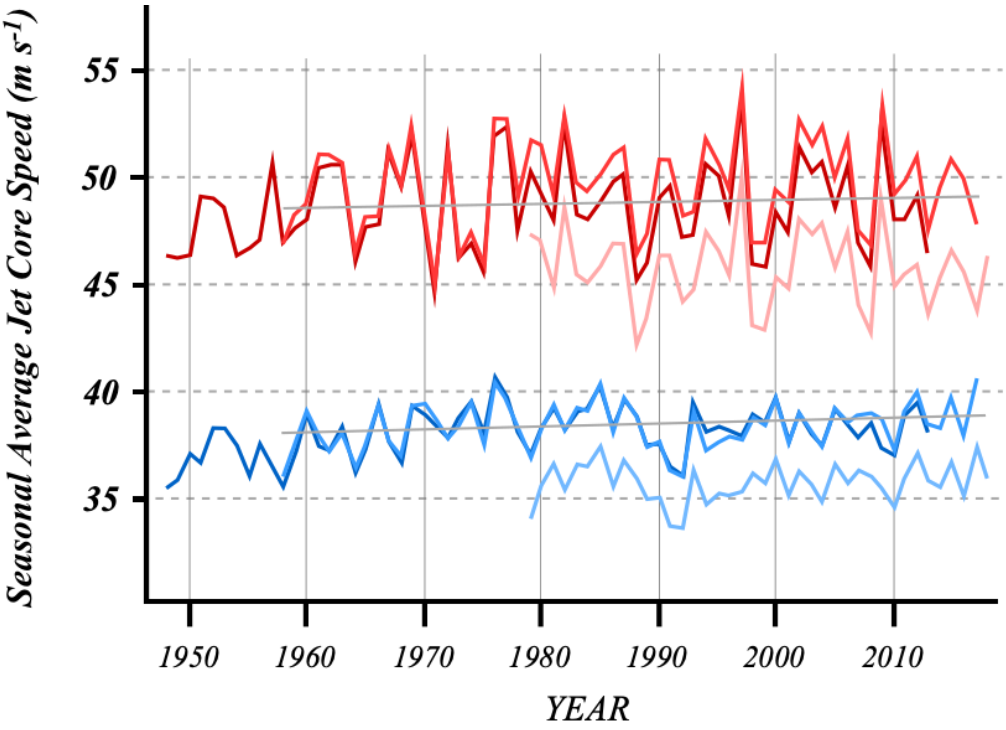

Fig. 8 Seasonal average **U** along the core isertel for the subtropical (red lines) and polar (blue lines) jets from each of the three reanalysis data sets. The light gray lines are trend lines for eachtime series
681 from the JRA-55 data.

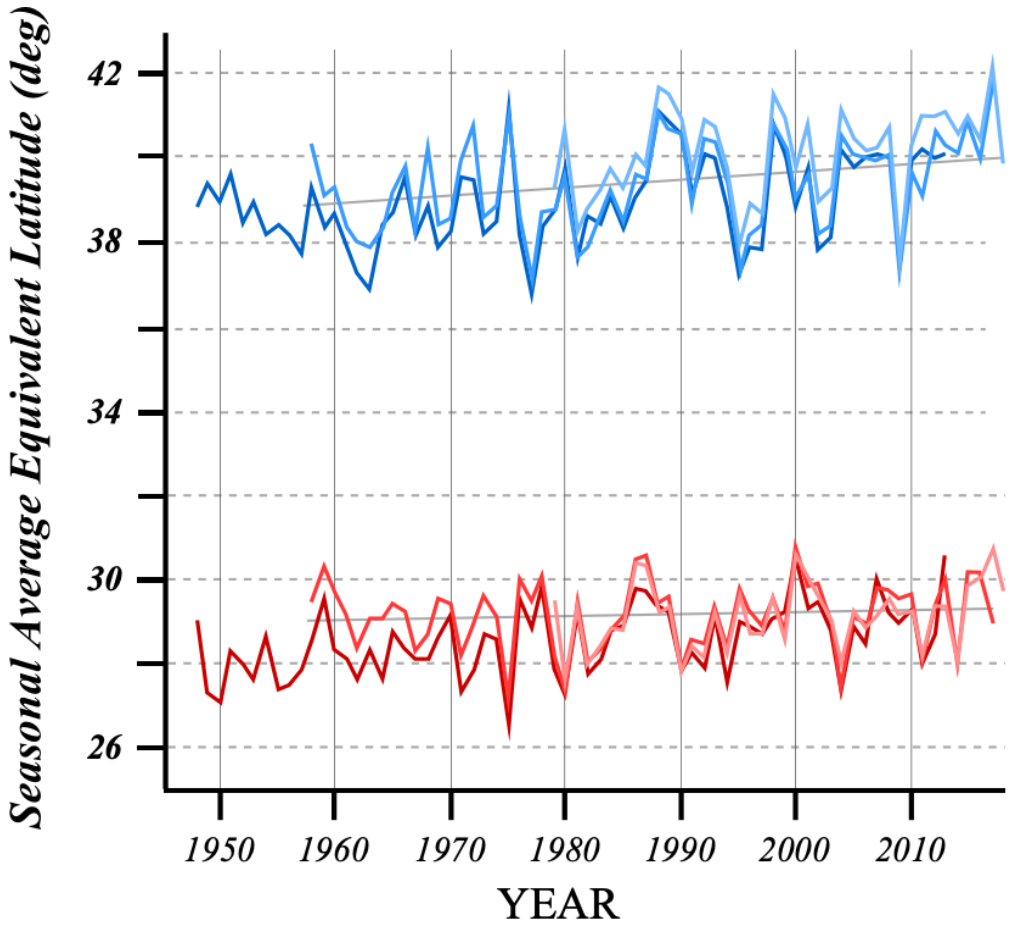

Fig. 9 Time series of the seasonal average equivalent latitude of the polar (blue lines) and subtropical (red lines) jets from the three different reanalysis data sets. The thin gray lines are the trend lines (from the JRA-55 data) which are small and only significant for the polar jet time series.

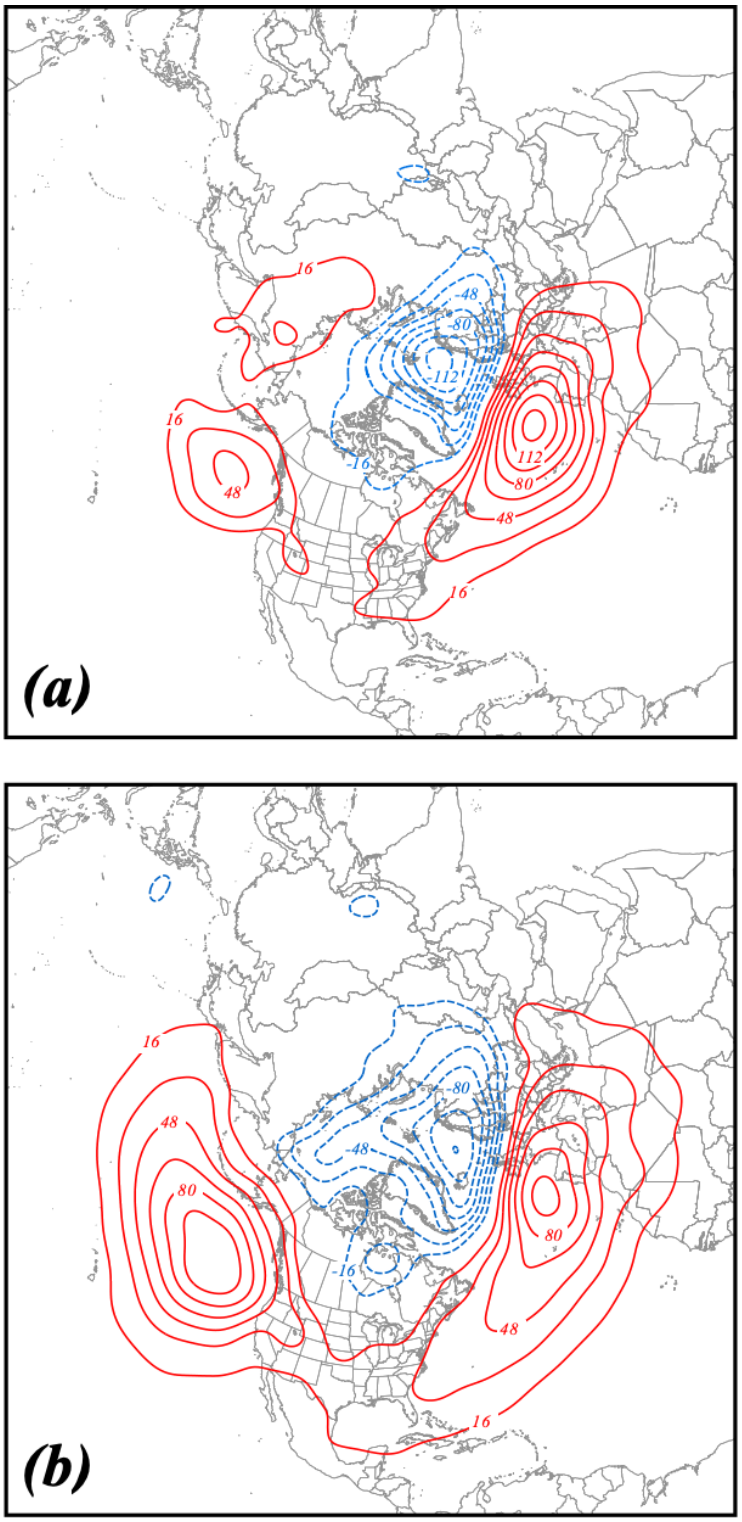

Fig. 10 1000 hPa height differences between composite waveist and least wavy (a) polar jet and (b) subtropical jet seasons. See Table 1 for identification of the specific years comprising each composite. Positive (negaitve) height differences are in solid red (dashed blue) lines, labeled in m and contoured every 16m (-16m) beginning at 16m (-16m).

683

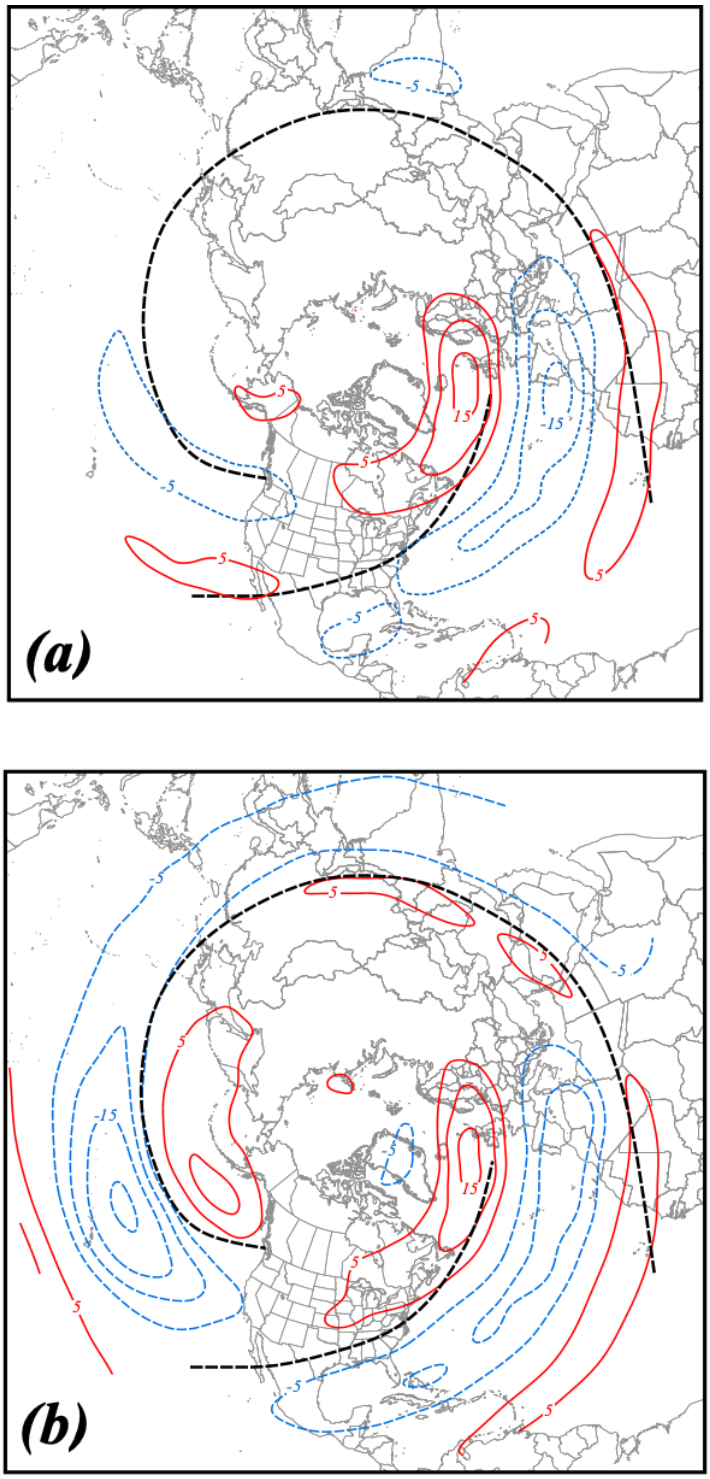

Fig. 11 300 hPa zonal wind differences between composite waviest and least wavy (a) polar jet and (b) subtropical jet seasons constructed from the NCEP/NCAR reanalysis. See Table 1 for identification of the specific years comprising each composite. Positive (negative) wind differences are in solid red (dashed blue) lines, labeled in m s^{-1} and contoured every 5 m s^{-1} (-5 m s^{-1}) beginning at 5 m s^{-1} (-5 m s^{-1}). Black solid lines represent climatological axes of the DJF 300 hPa zonal wind.

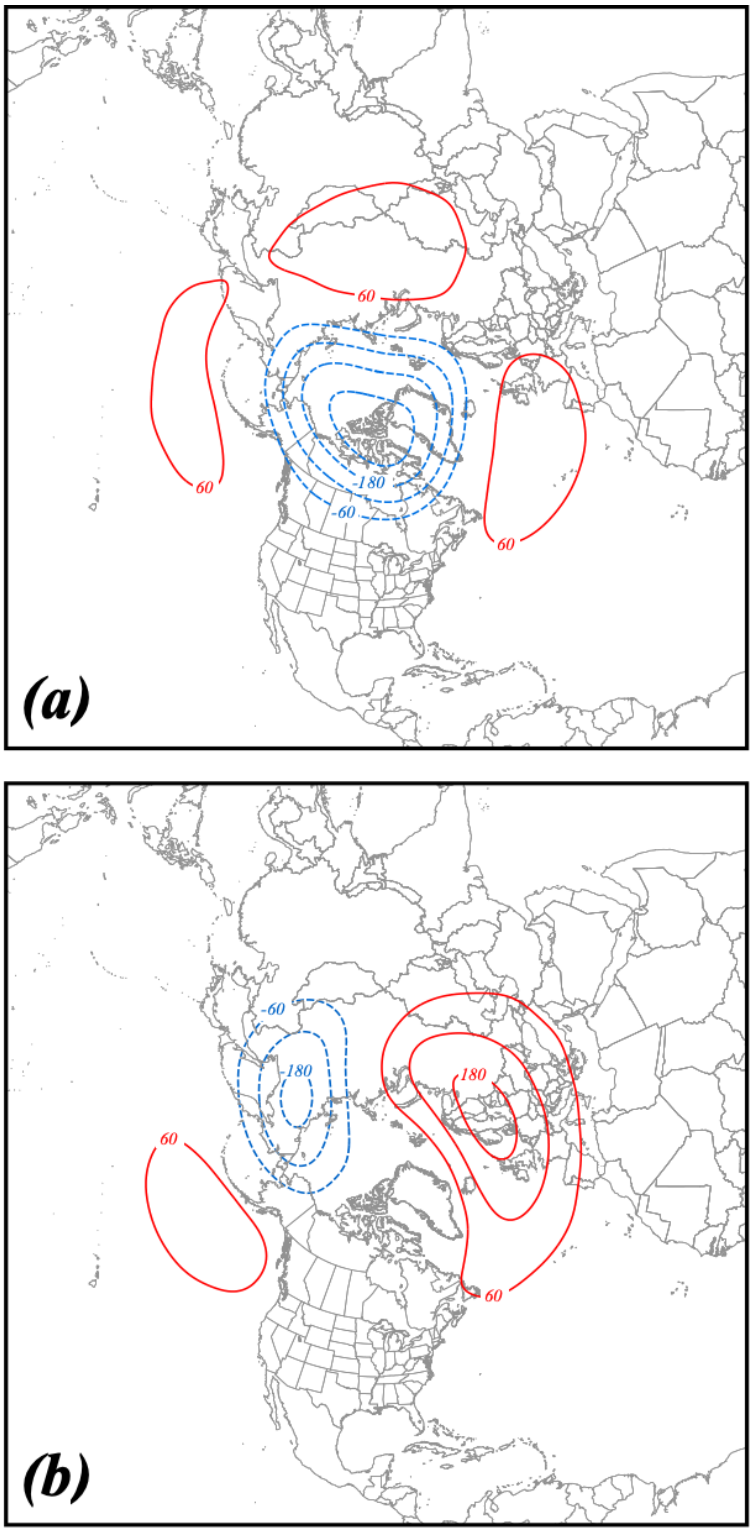

Fig. 12 50 hPa height differences between composite waviest and least wavy (a) polar jet and (b) subtropical jet seasons constructed from the NCEP/NCAR reanalysis. See Table 1 for identification of the specific years comprising each composite. Positive (negative) height differences are in solid red (dashed blue) lines, labeled in m and contoured every 60m (-60m) beginning at 60m (-60m).

685